Equivalent ionospheric currents for the 5 December 2006 solar flare effect determined from spherical cap harmonic analysis

L. R. Gaya-Piqué, J. J. Curto, J. M. Torta, Arnaud Chulliat

Equivalent ionospheric currents for the 5 December 2006 solar flare effect determined from spherical cap harmonic analysis

L. R. Gaya-Piqué,[1] J. J. Curto,[2] J. M. Torta,[2] and Arnaud Chulliat[1]

[1]   In this paper we analyze the prompt solar flare effect (SFE) associated to a strong X-ray flare that occurred on 5 December 2006 by using spherical cap harmonic analysis applied to the variations recorded in the European magnetic observatories network. The regional model allows the simultaneous modeling in space and time of the ionospheric equivalent current system responsible for the SFE, as well as for the regular diurnal variation S_R on that day. It is found that the SFE equivalent current system does not form as an enhancement of the S_R system. Its focus is distinct from that of the S_R, and it is located between 3 and 10° higher in latitude and circa 40 min later in local time.

Citation: Gaya-Piqué, L. R., J. J. Curto, J. M. Torta, and A. Chulliat (2008), Equivalent ionospheric currents for the 5 December 2006 solar flare effect determined from spherical cap harmonic analysis, *J. Geophys. Res.*, *113*, A07304, doi:10.1029/2007JA012934.

1.   Introduction

[2]   The influence of solar flares on the production of disturbances on the geomagnetic field recorded at the Earth's surface is a well known fact since its first observation by *Carrington* [1859] and *Hodgson* [1859]. Both authors correlated a contemporaneous prompt variation and a delayed magnetic storm as recorded at Kew Observatory with the observed brightening of the solar surface. However, the novelty of their discovery caused them to be cautious about establishing an unambiguous link between both phenomena. Many more observations were needed to establish a statistically significant direct connection between flares and geomagnetic irregular variations that were not established until the mid-20th century (see *Cliver* [1995] and references therein for a review). Now we know that the increase in the electromagnetic radiation that occurs during a solar flare produces changes in the ionospheric currents that result in concomitant short-lived perturbations in the geomagnetic field known as solar flare effects (SFE), whereas the shock wave caused by the arrival of solar plasma upon the magnetosphere is responsible for the geomagnetic storms some hours (or few days) after the occurrence of a solar flare.

[3]   Opposite to the worldwide, almost simultaneous character of geomagnetic storms, SFE are mainly restrained to the Earth's sunlit hemisphere. The equivalent current system responsible for the production of SFE is accepted to flow at a lower altitude than that of the regular diurnal variation (*Sq*) of the magnetic field [*Veldkamp and Van Sabben*, 1960; *Ohshio et al.*, 1967], and its focus has been generally found

located to the east (i.e., later in local time) with respect to the focus of the *Sq* system by using analytical approaches [*Van Sabben*, 1961; *Curto et al.*, 1994a]. A nonexhaustive list of works developed in the last century regarding SFE can be found in the work of *Rastogi et al.* [1999].

[4]   Not every SFE can be associated to a significant solar flare event, and not every flare provokes a rapid disturbance in the geomagnetic field. The radiation released during a solar flare spreads over the full electromagnetic spectrum, and it differs from one flare to another. Emissions containing a different range of frequencies produce diverse geomagnetic effects. *Curto and Gaya-Piqué* [2008] showed that the probability of generating a SFE increases when the flare spectrum presents a significant X-ray and H-α wavelength content, probably due to the fact that the ionizing effect of X-ray radiation on the lower ionosphere region is greater and therefore more efficient in SFE production.

[5]   Since flares are linked to other parameters (e.g., sunspots) that follow and define the 11-year solar activity cycle, the number of major flares is expected to reach a peak around the solar maximum and a trough for those years close to the solar minimum. However, in December 2006 (that is, at the end of solar cycle 23) the sunspot region number 10930 created a series of large X-ray flares as it rotated onto the visible solar hemisphere, causing major problems and blackouts in the Global Positioning System (GPS) network and the civil air navigation system, according to the Australian Space Weather Agency (http://www.ips.gov.au). Satellite GOES-13 (also damaged due to the incoming radiation) recorded a X9.0 flare on 5 December 2006 at 1018 UT that lasted for 27 min, reaching an intensity peak at 1035. Figure 1 shows the X-ray total energy content released during the phenomenon as recorded by GOES-12 satellite (data were downloaded from NOAA/NWS Space Weather Prediction Center Web site, http://www.swpc.noaa.gov). The integrated flux from the whole event was 0.71 J/m^2. San Vito observatory in Italy also

---

[1]Équipe de Géomagnetisme, Institut de Physique du Globe de Paris, CNRS, Paris, France.
[2]Observatori de l'Ebre, CSIC, Universitat Ramon Llull, Roquetes, Spain.
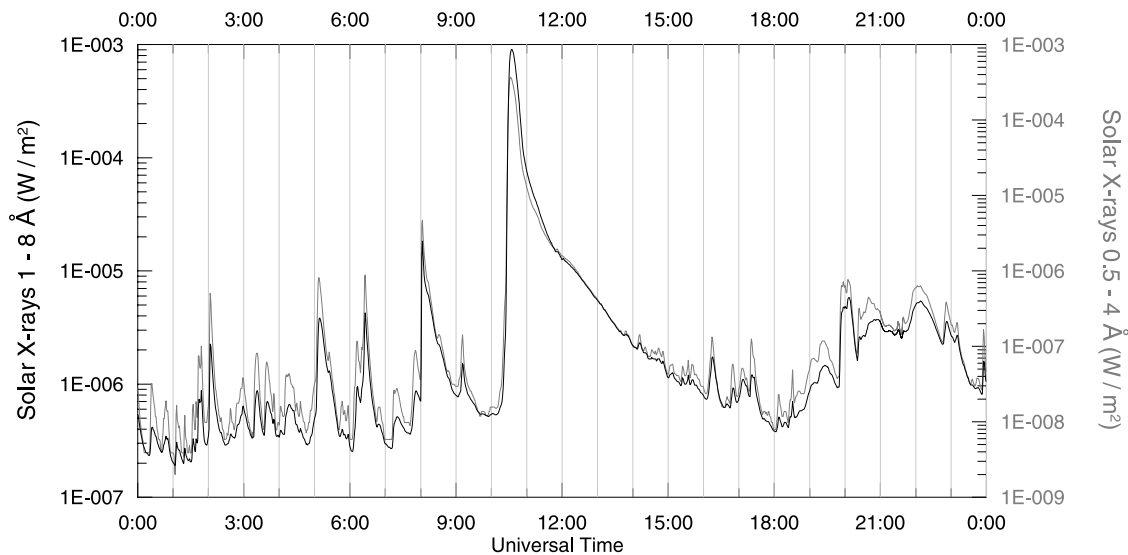
Figure 1. Solar X-ray flux in the 1–8 Å (black line) and 0.5–4 Å (gray line) ranges as measured by GOES-12 satellite for 5 December 2006.

reported an H-α flare of importance 2N starting at 1028 UT and ending at 1100 UT.

[6] Ebre Observatory, which houses the International Service on Rapid Magnetic Variations since 1975 [*Curto et al.*, 2007], received monthly reports from collaborating observatories pointing to a potential SFE starting at 1024 UT on 5 December 2006. A total of nine observatories first reported the event according to the Solar-Geophysical Data bulletin, published on a monthly basis by the NOAA National Geophysical Data Center Solar-Terrestrial Physics Division (available online at http://sgd.ngdc.noaa.gov). Figure 2 shows the three components of the magnetic field as recorded that day at Chambon-la-Forêt observatory (CLF; 48.0°N, 2.3°E geographic coordinates). The amplitude of that SFE reaches about 30 nT on the Y component, and it is the same order of magnitude as the regular *Sq* for this particular observatory. The fact that the magnetic field was

very quiet at the time of the SFE (Kp was equal to 0 for the three 3-h intervals prior to the event, and it did not exceed 2 h afterward until the end of the day) helped to clearly identify the phenomenon. It is also interesting to note that since the flare took place at the solar eastern limb and this effect depends on the particular Sun-Earth configuration, there was not a major geomagnetic storm linked to this event. However, *Futaana et al.* [2008] detected the effect of the coronal mass ejection associated to the solar flare close to Venus and Mars.

[7] The clarity of the SFE as observed at CLF contrasts with the fact that only a small percentage of observatories distributed worldwide reported the event. This is because not all magnetic observatories collaborate in detecting solar flare effects; moreover, not all the stations that provide the Rapid Magnetic Variations service with information about sudden storm commencements contribute to the identifica-
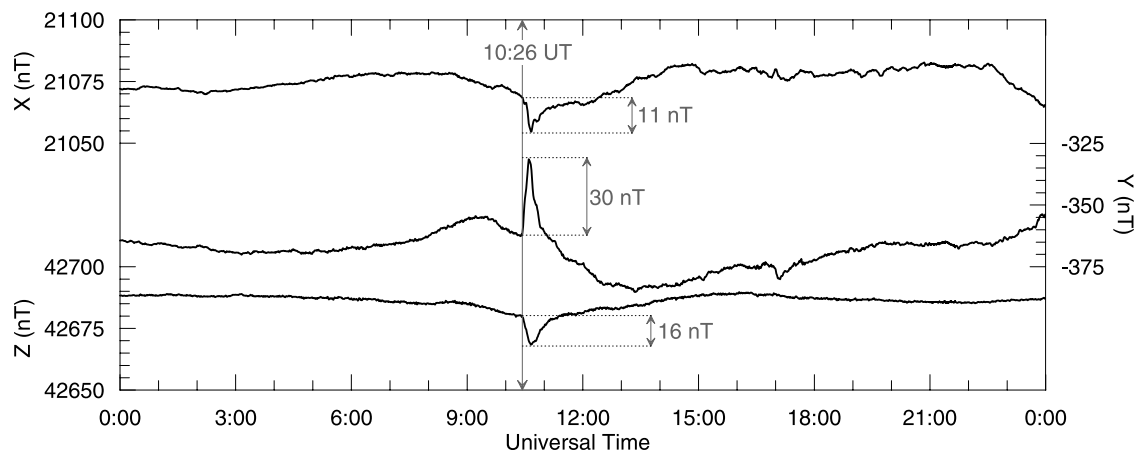
Figure 2. (top) X, (middle) Y, and (bottom) Z magnetic components recorded at Chambon-la-Forêt observatory on 5 December 2006. The maximum amplitude of the solar flare effect (SFE) is shown for each component.
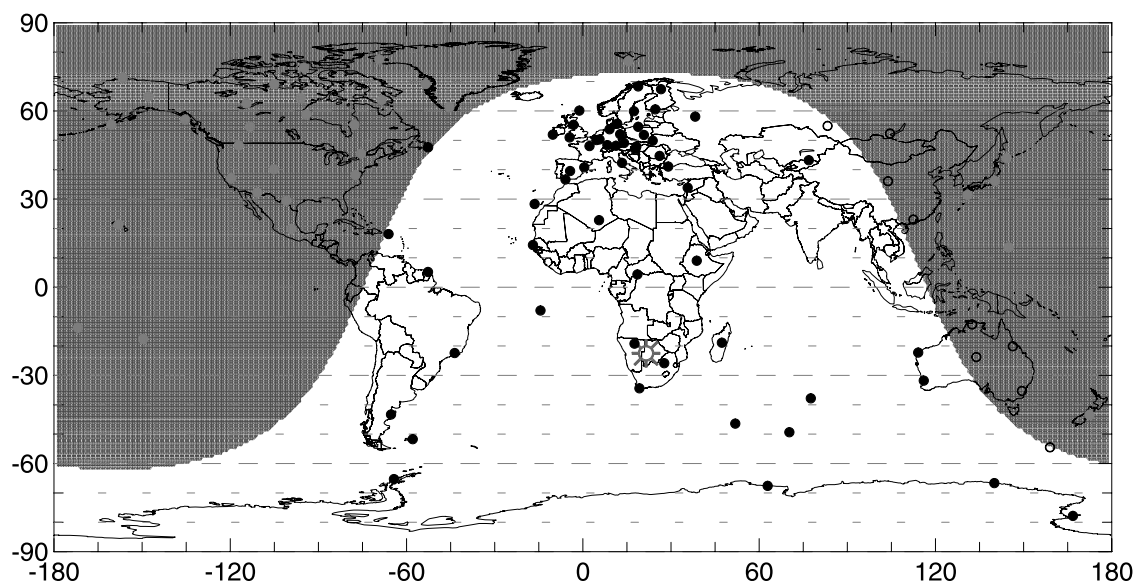
Figure 3. Spatial distribution of the Intermagnet observatories presenting minute data for 5 December 2006 as of September 2007. Black dots symbolize those observatories that clearly recorded the SFE, gray dots those that did not, and open circles represent those stations for which an unclear deviation in the magnetic field can be claimed at the moment of the event. The shaded area represents the dark hemisphere at the starting time of the phenomenon (1026 UT). The position of the subsolar point (approximately over Botswana) is also shown.

tion of SFE. Figure 3 shows the distribution of observatories belonging to the INTERMAGNET network (http://www. intermagnet.org) which provided 1-min magnetic values for the considered day (the list was last checked in September 2007). All magnetograms were visually inspected to check for those observatories where the SFE was clearly detected (black dots), those where a small movement is perceived but it is unclear (black circles), and those where the event was not seen at all (gray dots). As expected, the distribution of these three types of observatories clearly correlates with the night and day hemispheres, indicated in Figure 3 by the civil twilight terminator computed at 1026 UT, when the SFE starts to be visible in most of the observatories. Those observatories situated over the dawn terminator (San Juan in Puerto Rico and Saint John's in Canada) detected the SFE since they were inside the sunlit hemisphere a few minutes after the starting time of the event, as opposed to those observatories located over the dusk terminator. It is also worth noting that those observatories located over the northern auroral oval, especially those in Canada and Alaska, presented some intense magnetic activity starting approximately 1 h before the occurrence of the X9.0 solar flare.

[8] The usual problem of the uneven worldwide distribution of observatories clearly arises also in this case after a look to Figure 3. Moreover, since SFE are mainly hemispherical phenomena, although evidence for SFE to be found in the dark hemisphere was claimed by *Sastri* [1975], the difficulties to conduct a global study on the equivalent currents that produce the solar flare effects are even more important.

[9] In this paper we present a regional approach for the study of these current systems by using spherical cap harmonic analysis (SCHA). Our goal was the characterization

of the currents that created the particular SFE on 5 December 2006 over the European sector. As will be shown, the SCHA technique allows for a simultaneous temporal and spatial approach to the problem, so the evolution of the phenomena can be followed in a continuous manner. We introduce in the next section the data employed and the method used to separate the SFE rapid deviation from the regular daily variation for each observatory. Section 3 presents the SCHA technique and a discussion on the internal-external separation issue. The expressions to obtain the shape of the ionospheric equivalent currents from an ensemble of spherical cap harmonic coefficients, and a test on synthetic data are introduced in section 4. Section 5 presents the SCHA models of the equivalent current systems for the SFE under study and for the daily regular variation on 5 December 2006. The paper finishes with a discussion of our results compared to other previous works conducted on an analytical mode.

2. Data Used and Isolation of SFE

[10] The considered SFE took place around local noon for central Europe. Conducting our study over the European region is advantageous because of the midlatitudinal location of the continent. Moreover, the density of observatories is much higher there compared to any other area in the world. Figure 4 shows the location of the stations considered here (located inside the cap represented by the black contour). Only stations presenting three-component magnetic field data were considered.

[11] The amplitude of the SFE variation at each individual observatory was derived after computing the difference between the recorded magnetic values and a plausible regular variation obtained through polynomial interpolation of the real magnetic data before and after the SFE event.
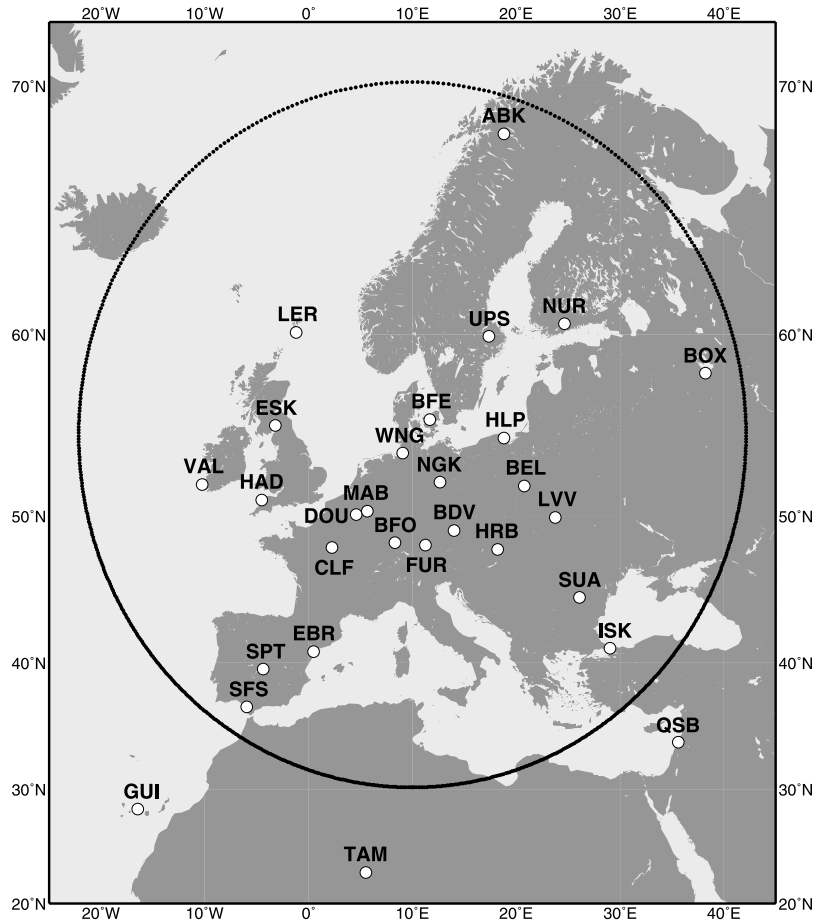
Figure 4. Location of the observatories considered in this study. The black circle represents the border of the spherical cap for which the model for the SFE is valid.

Each component of this regular variation was therefore expressed as a temporal series expansion in the form:

$$S_R(t) = \sum_{q=0}^{Q} b_q \left(\frac{t - t_0}{T}\right)^q \tag{1}$$

where t_0 and T are the translational and scaling parameters, and q the degree of each polynomial term, with a maximum degree Q. Figure 5 shows the magnetic field (thick black lines) recorded between 0900 and 1500 UT at four different observatories that cover a wide geographical area (especially in longitude): Borok (BOX; 58.1°N, 38.2°E), Furstenfeldbruck (FUR; 48.2°N, 11.3°E), San Pablo–Toledo (SPT; 39.6°N, −4.4°E), and Valentia (VAL; 51.9°N, −10.3°E). Figure 5 also presents the different approaches tried in order to interpolate the regular diurnal variation. The thin black line represents the external field predicted by Comprehensive Model version 4 (CM4) [*Sabaka et al.*, 2004] for the parameters that characterized the magnetic field activity on 5 December 2006. Values of *Dst* and F10.7 indices were respectively downloaded from the World Data Center for Geomagnetism in Kyoto (http://swdcwww.kugi.kyoto-u.ac.jp/index.html) and the Solar-Terrestrial Physics Division of NOAA (http://www.ngdc.noaa.gov/stp). Even though the fit given by CM4 is quite good, it is not accurate enough for an exact representation of the S_R for this particular day. This is due to the fact that the regular solar quiet diurnal variation for a particular day, S_R, differs from the average solar quiet diurnal variation, *Sq*, represented by CM4, and also to the provisory (quick look) character of the magnetic activity indices used to compute the daily variation from CM. The dotted black line in Figure 5 represents the regular diurnal variation as computed from the five quietest days of November and December 2006 for each individual observatory. For some observatories, there is a good agreement between this averaged diurnal variation and the real recorded field before and after the event, as 5 December was classified as the ninth quietest day (Q9) of the month. However, in most of the cases there is a low compatibility between mean and real diurnal variation (see for example the differences in the Z component for BOX and in the X component for SPT), due to the day-to-day variability of the solar quiet variation.

[12] Since none of these alternatives (CM4 and the use of quietest days) gave satisfactory results, we decided to carefully interpolate the data using polynomials (thick white lines in Figure 5) in order to obtain a regular diurnal variation for the time of the event. A different polynomial degree was used for each component and station. Interpolated values were compared with the shape of the averaged regular variation previously computed. This comparison helped in choosing the SFE end time, and the maximum polynomial degree expansion for each individual station.
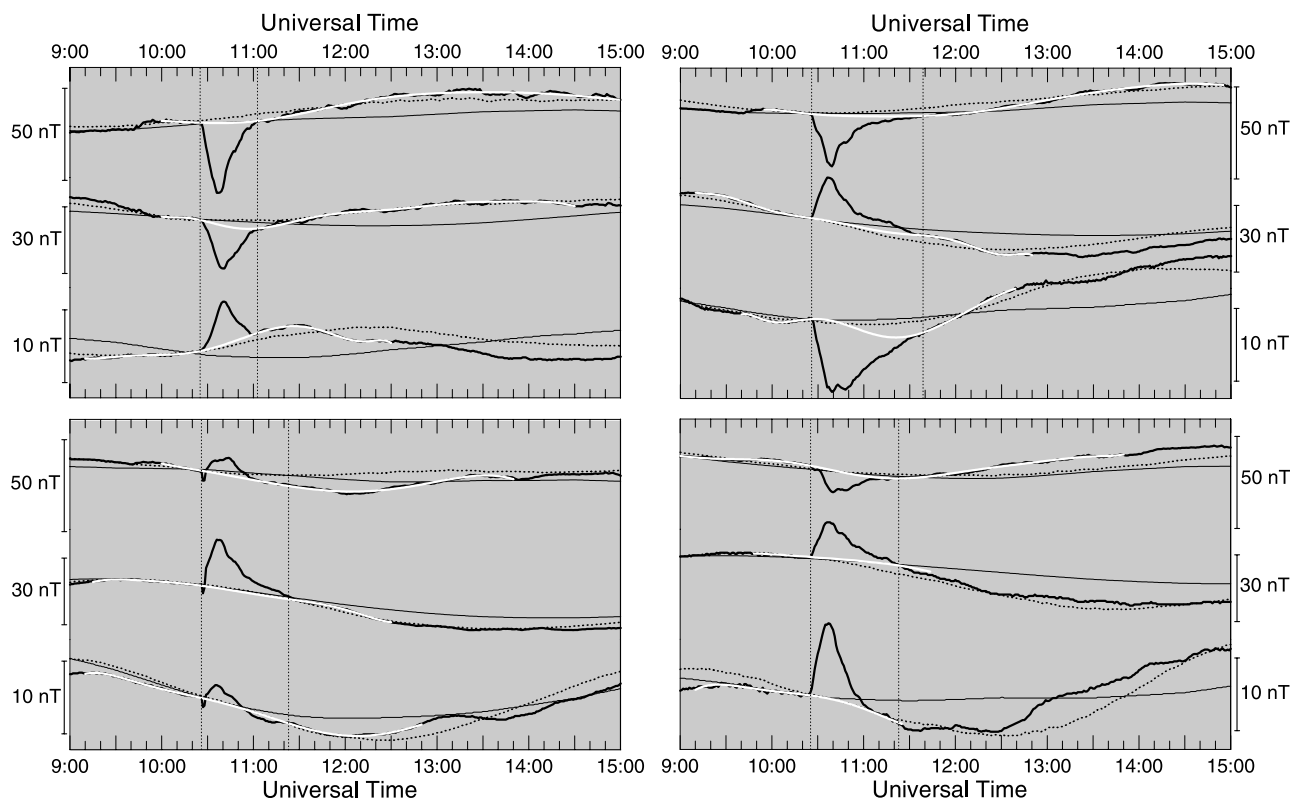
Figure 5. Magnetograms corresponding to Borok (BOX; top, left), Furstenfeldbruck (FUR; top, right), San Pablo-Toledo (SPT; bottom, left), and Valentia (VAL; bottom, right) observatories for 5 December 2006 between 0900 UT and 1500 UT. Inside each box, thick black top curves correspond to X component, middle ones to Y component, and bottom ones to Z component. Thick white curves represent the values of the regular diurnal variation obtained by polynomial interpolation for the time of the SFE. Dotted black lines represent the averaged diurnal variation for the five quietest days of November and December 2006. Thin black curves correspond to the external field variations predicted by CM4 model.

For the particular cases presented in Figure 5, the maximum degree for the polynomial interpolation goes from $Q = 5$ for the X component as recorded at SPT up to $Q = 10$ for the three magnetic components from BOX. A shift in the end time for the event entails a change in the interpolated function, therefore a change in the obtained regular variation, and a different amplitude for the SFE, especially for the last part of the event, when the change in slope would be more pronounced. The decay structure of a SFE is typical of a system with small inertia (the recombination coefficient for electrons belonging to the ionospheric E, and especially D regions is high enough to maintain the additional electronic density during only few minutes after the decay of the ionization source), so no long-term decay trends are expected after the flare radiation fall to the regular level. The diurnal variation obtained by polynomial interpolation realistically represents the expected diurnal variation, as shown in Figure 5. The mean duration of the event as computed from the magnetograms of the 26 stations considered in this study was around 60 min, with a standard deviation of 20 min. The event clearly lasted for less than 45 min at 10 of these observatories.

[13] The amplitude of the SFE was found from difference between the recorded field and the interpolated curve, this difference being positive in those cases where the SFE

represented an increase in the absolute value of the field and negative vice versa. We assumed that these differences were exclusively due to the ionospheric currents created by the SFE phenomenon. It is equivalent to assume that the magnetospheric field changed little over the duration of the SFE. In case of a substantial change of the magnetospheric field, the variation produced by the SFE on the magnetic field would be probably masked by the variations of magnetospheric origin, so it would be difficult to isolate and study these phenomena. The differences, sampled at 1-min interval from 1026 UT until the end time for the event at each particular station, were used as input data to model the equivalent ionospheric current system for the SFE, whereas the interpolated curve was used as input to obtain a model for the regular variation.

3. Spherical Cap Harmonic Analysis and the Internal-External Separation

[14] Spherical cap harmonic analysis (SCHA) [*Haines*, 1985] has probably been the most used regional modeling technique for all kinds of geomagnetic studies over the last two decades (see *Torta et al.* [2006, Table 1] for a comprehensive review of English-written works related to SCHA as of May 2005). It is based on the solution of the Laplace

equation over a bounded regional cap of half-angle θ_0:

$$V(r, \theta, \lambda) = a \sum_{k=0}^{K_i} \sum_{m=0}^{k} \left(\frac{a}{r}\right)^{n_k+1} \left(g_k^{m,i} \cos m\lambda + h_k^{m,i} \sin m\lambda\right)$$
$$\cdot P_{n_k}^m(\cos \theta) + a \sum_{k=1}^{K_e} \sum_{m=0}^{k} \left(\frac{r}{a}\right)^{n_k}$$
$$\cdot \left(g_k^{m,e} \cos m\lambda + h_k^{m,e} \sin m\lambda\right) \cdot P_{n_k}^m(\cos \theta) \qquad (2)$$

$g_{n_k}^m$ and $h_{n_k}^m$ are the spherical cap harmonic coefficients that define the internal and external potential, represented in equation (2) either by the superscript i or e, respectively. The associated Legendre functions $P_{n_k}^m(\cos \theta)$ satisfy arbitrary boundary conditions at the edge of the cap, giving rise to noninteger degrees n_k, where k is an ordering index that increases with m. When $\theta_0 = 180°$, equation (2) reduces to the usual global spherical harmonic solution for the potential with maximum expansion degree equal to K_i for internal fields and K_e for external fields. In case the model is intended to represent not only the spatial but also the temporal behavior of the field, a temporal expansion is added to these coefficients up to a maximum degree L_{max}.

[15] The theoretical ability of SCHA to separate between internal and external fields makes it an attractive tool for the study of geomagnetic variations of external origin and for the characterization of ionospheric sources. *Haines and Torta* [1994] used SCHA to model the magnetic variations for a very quiet geomagnetic day in order to compute the equivalent currents, that is, those ionospheric and induced currents able to represent the measured variations of the geomagnetic field. *Torta et al.* [1997] applied SCHA at a later stage to investigate the behavior of the *Sq* currents over Europe for some selected quiet days over a minimum magnetic activity period. As in the work of *Haines and Torta* [1994], the regional pattern of the *Sq* focus and its temporal and spatial variations were properly represented, and the displacement of the ionospheric currents system was monitored in detail through the surface of the cap with temporal continuity. The fact that (due to the radial dependency in equation (2)) external and internal sets of coefficients contribute in a different way to the field at different altitudes helps in the separation of the fields. More recently, *Kotzé* [2002] made use of SCHA to identify the external field when analyzing Ørsted satellite total intensity field data over southern Africa. The external contributions were modeled as a general function in longitude and colatitude over the surface of the spherical cap. The SCHA expansion of the function was truncated at $K_e = 1$, so three coefficients were derived to give account of the external field for each satellite measurement.

[16] Even though these studies demonstrated SCHA to be useful when representing the kinematics of the ionospheric current system at a regional scale, the method presents limitations in the internal-external discrimination. *Torta et al.* [1992] found that the use of internal and external coefficients improved the fit to a synthetic input data set consisting of only internal contributions. *Torta and De Santis* [1996] showed that in spite of a good representation of the overall field by the full set of coefficients when modeling the current functions over Europe, internal and external coefficients were not able to describe properly the respective contributions

when used separately. Nevertheless, since the real and the modeled variations were approximately in phase, they concluded that the information obtained about the motion of the ionospheric current systems was still valid.

[17] Moreover, the authors proposed to still use SCHA when the cap under study had a similar size to that of the area in which the geomagnetic variations take place, in order to have the same inherent wavelength characteristics for the input and the model output data. An improvement in the field separation was in fact achieved when artificially enlarging the size of the cap. However, the cap cannot be expanded ad infinitum when data only cover a small central part of the region. This is because of the nonorthogonality of the basis functions over the considered region, and the numerical instabilities associated to the solution of the poorly conditioned normal matrix. A possible explanation for the necessity to increase the size of the cap comes from the fact that an internal-external separation may be equivalent to independently modeling the horizontal components on the one hand, and the radial component on the other [*Lowes*, 1999; *Gaya-Piqué*, 2004, section II.3]. *Torta et al.* [1992] showed that the smaller area for which the model is developed, the more difficult is to simultaneously represent X, Y, and Z, so moving toward bigger size caps would solve the joint fit of vector data as well as the issues related to internal-external separation.

[18] Recently, *Thébault et al.* [2006] proposed a revised version of the spherical cap harmonic analysis (R-SCHA) by solving the Laplace equation over a spherical cone instead of on a spherical cap. The new surface and boundary conditions involved an extra set of basis functions (Mehler or conical functions) to the solution. The main ability of R-SCHA compared with SCHA is its ability to represent the spatial variation of the magnetic field inside the conical domain, provided that data are available at its upper and lower boundaries. The authors devoted a full section to the problem of the internal-external separation. Equations (28) to (31) in the work of *Thébault et al.* [2006] show that there is a lack of meaning in the internal-external spherical cap coefficients when considered individually. These equations demonstrate that both internal and external sets are necessary in order to represent the field using SCHA, even when input data only contain signal from either internal or external sources. As stated by *Thébault et al.* [2006], a proper technique to perform regional internal-external field separation is still missing.

[19] The apparent validity of the obtained results when the technique is used cautiously, as presented in the previous paragraphs, gave us confidence (taking all the necessary care to interpret our results) to apply spherical cap harmonic analysis to model the magnetic variation associated with the solar flare. In what follows we present the equations that describe the SCHA equivalent current functions and an example using synthetic data of the internal-external separation provided by SCHA.

4. Equivalent Current Functions and Synthetic Case

[20] *Haines and Torta* [1994] provided the formulation for computing the equivalent current densities and equivalent current functions for the spherical cap analysis. The authors

pointed out that previous works either did not show the right formulations [*Walker*, 1989] or did not give the equations at all [*Langel*, 1993]. The ionospheric equivalent current functions responsible for the variations in the magnetic field recorded at the surface are given by the expression:

$$\Psi_{ionos}(\theta, \lambda) = -\frac{a}{\mu_0} \sum_{k=1}^{K_e} \sum_{m=0}^{k} \frac{2n_k + 1}{n_k + 1} \left(\frac{r}{a}\right)^{n_k}$$
$$\cdot \left(g_k^{m,e} \cos m\lambda + h_k^{m,e} \sin m\lambda\right) \cdot P_{n_k}^m(\cos\theta) \quad (3)$$

[21] These currents are confined to a spherical surface of radius $r = R_E + h$, where h is the altitude above the Earth's surface R_E. Assuming that the ionization responsible for the SFE variation takes place mainly in the lower ionospheric E region [e.g., *Veldkamp and Van Sabben*, 1960], the value for h is fixed at 100 km and the currents are only evaluated for this shell (for some of our tests the altitude was fixed at 90 km, the boundary between ionospheric D and E layers, without a noticeable change in the shape of the current system). When n_k is an integer, then $k = n$ and $n_k = k$, and equation (3) is equivalent to the one used in global spherical harmonic analysis, already given by *Chapman and Bartels* [1940]. Note that equation (3) does not depend on the peculiar g_0^0 spherical cap harmonic coefficient. As pointed out in the introduction, this approach allows for a simultaneous spatial and temporal discrimination of the equivalent currents provoked by the increase in ionization associated with the solar flare, as opposed to classical studies [e.g., *Curto et al.*, 1994a] where the external equivalent current vector was taken as simply a rotation of the external horizontal activity vector (about two thirds of the total variation present in the horizontal vector).

[22] In order to check the validity of the approach and the capability to separate internal from external contributions, a study was conducted on synthetic data obtained from CM4 model. This case study was conducted on Sq data since in this way it was possible to directly compare the output model with the synthetic input data. An ionospheric field obtained as the sum of the primary and induced contributions synthesized by CM4 model was computed at the locations of the observatories given in Figure 4, and also at auxiliary points located 15 degrees eastward and westward of each station but at the same dip latitude. This approach was already used by *Torta et al.* [1997] to augment the data coverage over the spherical cap, since the diurnal variation is almost a local-time phenomenon. This approach assumes that a station "A" located 15° east of a station "B" records the same shape and amplitude for the diurnal variation as "B" but one hour in advance, and correspondingly a station "C" located 15° west of "A" presents the same diurnal variation but with 1-h delay.

[23] A SCHA model was developed on a 45° cap centered at 45°N, 10°E using the above synthetic CM4 values as input data. The maximum spatial and temporal expansion for the model were $K_{int} = K_{ext} = 4$ and $L_{max} = 4$, respectively, using Fourier series as temporal basis functions. Figure 6 shows the equivalent currents computed applying equation (3) on the external coefficients of the obtained SCHA model (continuous line), compared to the E region equivalent currents for the primary ionospheric field computed directly from the CM4 model, equation (54) of

Sabaka et al. [2002], on a regular grid (dashed line). As can be seen, the shapes of the equivalent current systems are very similar, especially close to the center of the cap (represented by the black circle), so it can be assumed that SCHA separates the internal from the external contributions with rather reliability, at least for the Sq variation, for this particular data distribution and model parameterization.

5. Results and Discussion

[24] Several model parameterizations were attempted to represent the SFE variations and therefore to characterize the external equivalent current system. The different tests included modifying the size of the cap, the temporal basis functions adopted, and the maximum spatial and temporal expansion degrees. It is not possible to apply in this case the data triplication approach used for the S_R to ensure a better coverage of the area, since the SFE is a UT-based phenomenon. A spherical cap of 20° half-angle centered at 50°N, 10°E was chosen. This cap embraces a total of 26 INTER-MAGNET observatories over Europe providing data for 5 December 2006. Caps of bigger size were considered, in order to include three observatories located below 35°N (Guimar, GUI, 28.3°N; Tamanrasset, TAM, 22.8°N; and Qsaybeh, QSB, 33.9°N), and to check whether, as pointed out before, the enlargement of the cap affected positively the internal-external separation. However, a bigger cap resulted in too large areas lacking in magnetic stations, and the 20° cap produced realistic equivalent current functions. Polynomial series were used as temporal basis functions representing the evolution of the variation between T = 0 min (corresponding to 1026 UT on the studied day) and T = 120 min (when it can be affirmed that the magnetic field is back to its regular shape as if no SFE existed). No considerable differences were found when using other types of basis functions; the polynomial expansion set the amplitude of the SFE equal to zero at the end of the considered period for most of the observatories. Finally, the maximum values chosen for the spatial expansion in equations (2) and (3) were $K_i = K_e = 4$, and $L_{max} = 8$ was chosen for the temporal expansion. A compromise between fit of the model to the data and realistic representation of the currents was sought. Going to higher degree expansions improved the fit, but at the expense of a bad-posed normal matrix that led to overfitting the input data and to unrealistic shapes for the equivalent currents (due to the high values of the spherical cap coefficients that try to compensate each other). A stepwise regression process based on the statistical F test was applied to obtain the coefficients of the model [*Haines and Torta*, 1994].

[25] Figure 7 shows the external equivalent current function derived from the final SCHA model by applying equation (3). The equivalent currents flow along these contour lines. The black circle delimits the cap area inside which the model is valid. The white arrows represent the horizontal component of the magnetic variation associated to the SFE at each observatory for a given snapshot, with magnitude and phase derived as:

$$|Sfe_H| = \sqrt{\Delta X^2 + \Delta Y^2} \quad , \quad \alpha_{Sfe_H} = \tan^{-1}\left(\frac{\Delta X}{\Delta Y}\right) \quad (4)$$
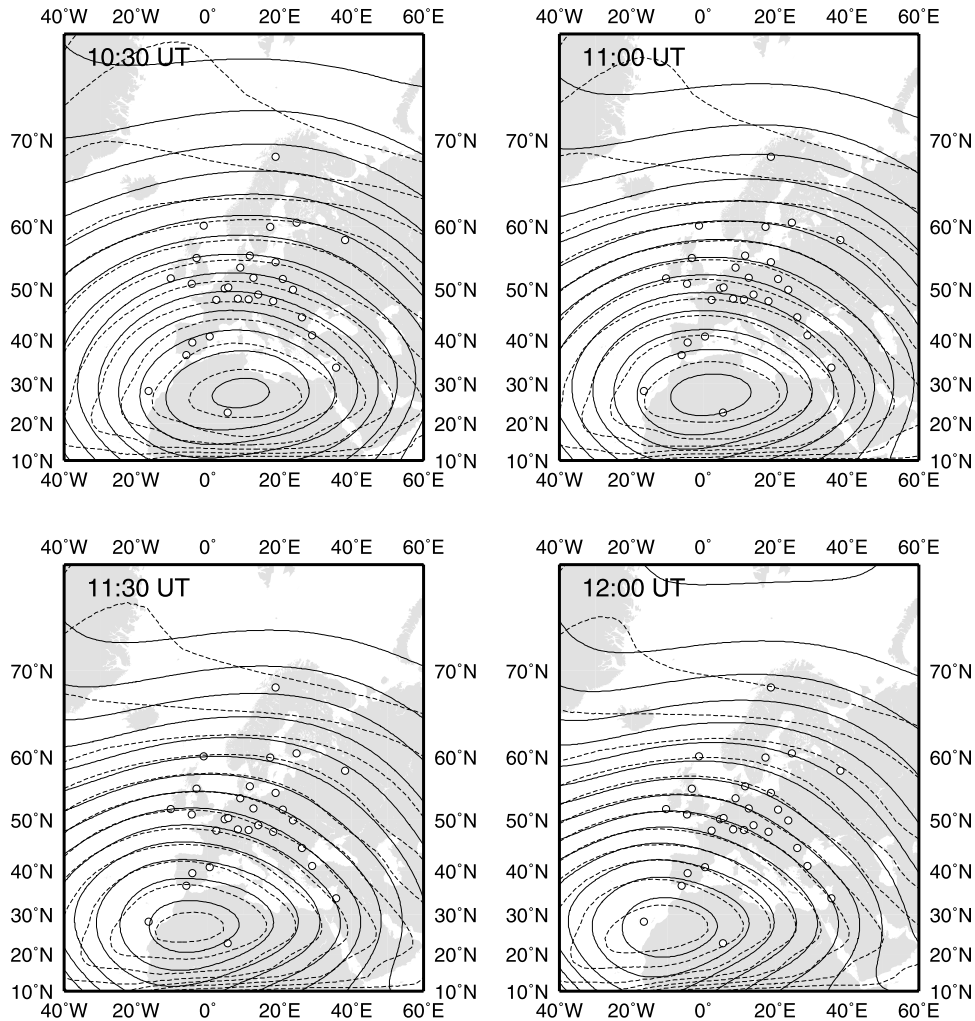
Figure 6. Continuous line: external equivalent current systems determined from a spherical cap harmonic analysis (SCHA) model using primary (external) and induced (internal) ionospheric magnetic field values from CM4 as input data. Dashed line: primary (external) equivalent current systems as given by CM4 [*Sabaka et al.*, 2004] for the same day. The synthetic CM4 values used as input data to obtain the SCHA model were generated at the real observatories locations marked by the solid circles as well as at locations at the same dip latitude but shifted $+15°/-15°$ in longitude with respect to the real observatories. Contour interval is 5 kA for both current systems.

being ΔX and ΔY the amplitude of the recorded SFE in the north and east components of the magnetic field, respectively. Note that they correspond to the total (external plus internal) field measured at each station. As stated by *Curto et al.* [1994b], the induced currents for both Sq and SFE amount about 40% of the total intensity, so the isolation of the primary currents by the SCHA model allows for a more accurate determination of the focus position (assuming that the internal-external separation has been done properly). The figure also shows the external equivalent current function for the regular variation S_R obtained through another SCHA model. This method was preferred to the representation of the Sq as given by CM4 because of the reasons given in section 2, and after considering the good results described in section 4 for the synthetic case. The SCHA model for the S_R variation was obtained using the interpolated regular diurnal variation curve obtained in

section 2 between 0830 UT and 1330 UT as the input data. Values from the real observatories shown in Figure 4 were considered, as well as 1-h shifted values at locations displaced $15°$ in longitude, as explained in section 4. The model was developed on a 45 degree cap centered at 45°N, 10°E. We also tried a model for the S_R using the same cap that was considered for the modeling of the SFE currents. The position of the vortex does not change at all, and only the shape of the currents changes slightly, especially for the NW part of the cap and of course outside the boundaries of the smaller cap. The maximum spatial and temporal expansions adopted were $K_{int} = K_{ext} = L_{max} = 4$, using Fourier series as temporal basis functions. The focus of the S_R deduced from the SCHA model is located to the north compared to the Sq focus that would be obtained if CM4 were used. We obtained a mean difference of about $10°$ in latitude and $2°$ in longitude (i.e., the SCHA S_R focus is
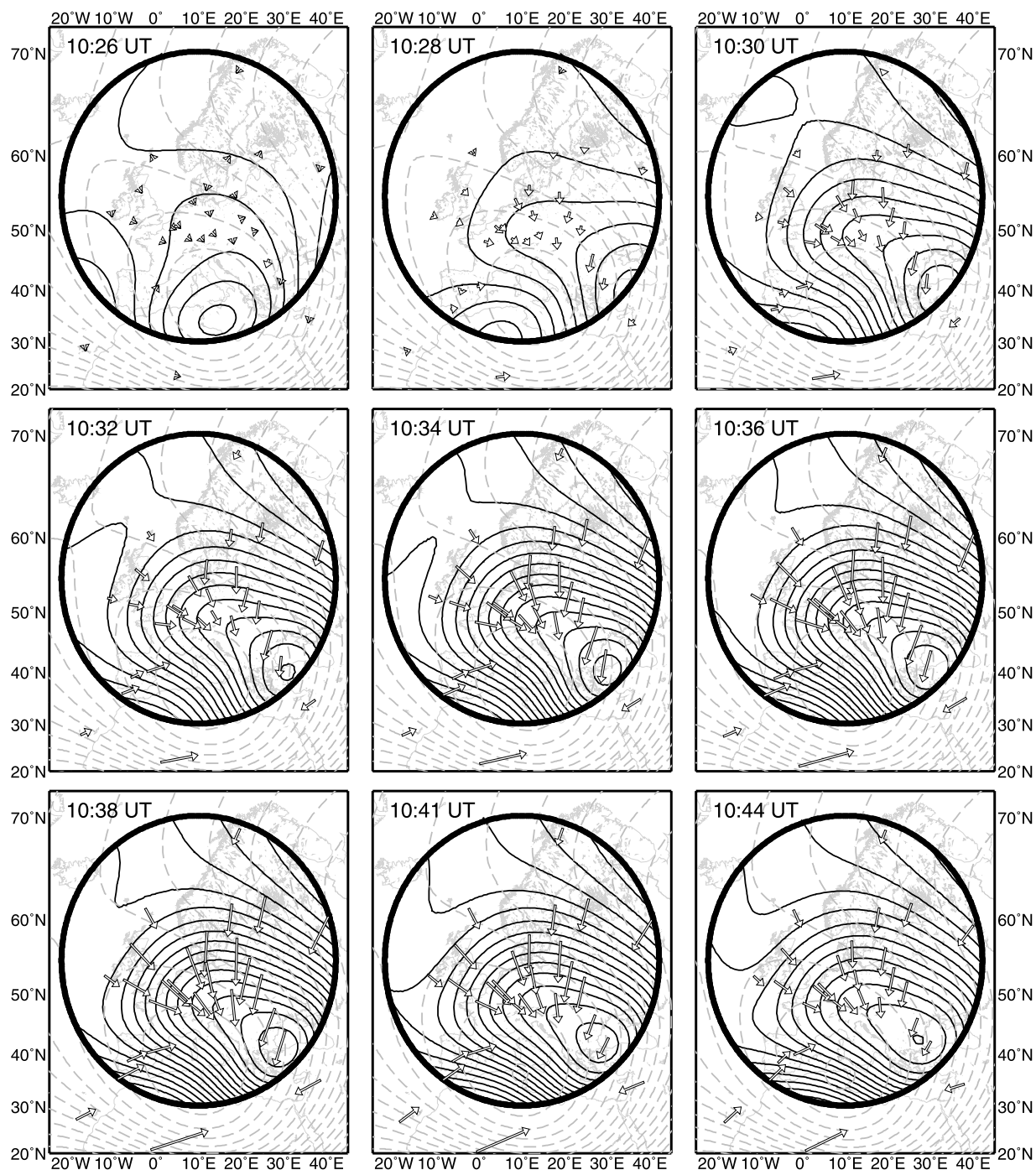
Figure 7. SFE equivalent current system (black continuous contour lines) created by the solar flare under study as given by the SCHA model for different moments. The position of the S_R focus (gray dashed contour lines) as computed through a different SCHA model is also shown for each particular snapshot. Contour interval 5 kA for both current systems. The arrows represent the horizontal SFE vector as recorded at each particular observatory.

found to the northeast with respect to the CM4 Sq focus). The difference is again attributed to the day-to-day variability of the ionospheric current system. An evaluation of the change in the Sq system for different magnetic universal times and seasons can be found in the work of *Sabaka et al.* [2002]. The fact that the flow lines do not close around the focus for the NW part of the considered region may be due to the lack of data in the area compared to the size of the considered cap. The contour spacing in Figure 7 represents a 5 kA current flux for both SFE and S_R systems. The currents mainly flow in counterclockwise sense around the foci, as typically corresponds to the overhead northern hemispherical Sq system.
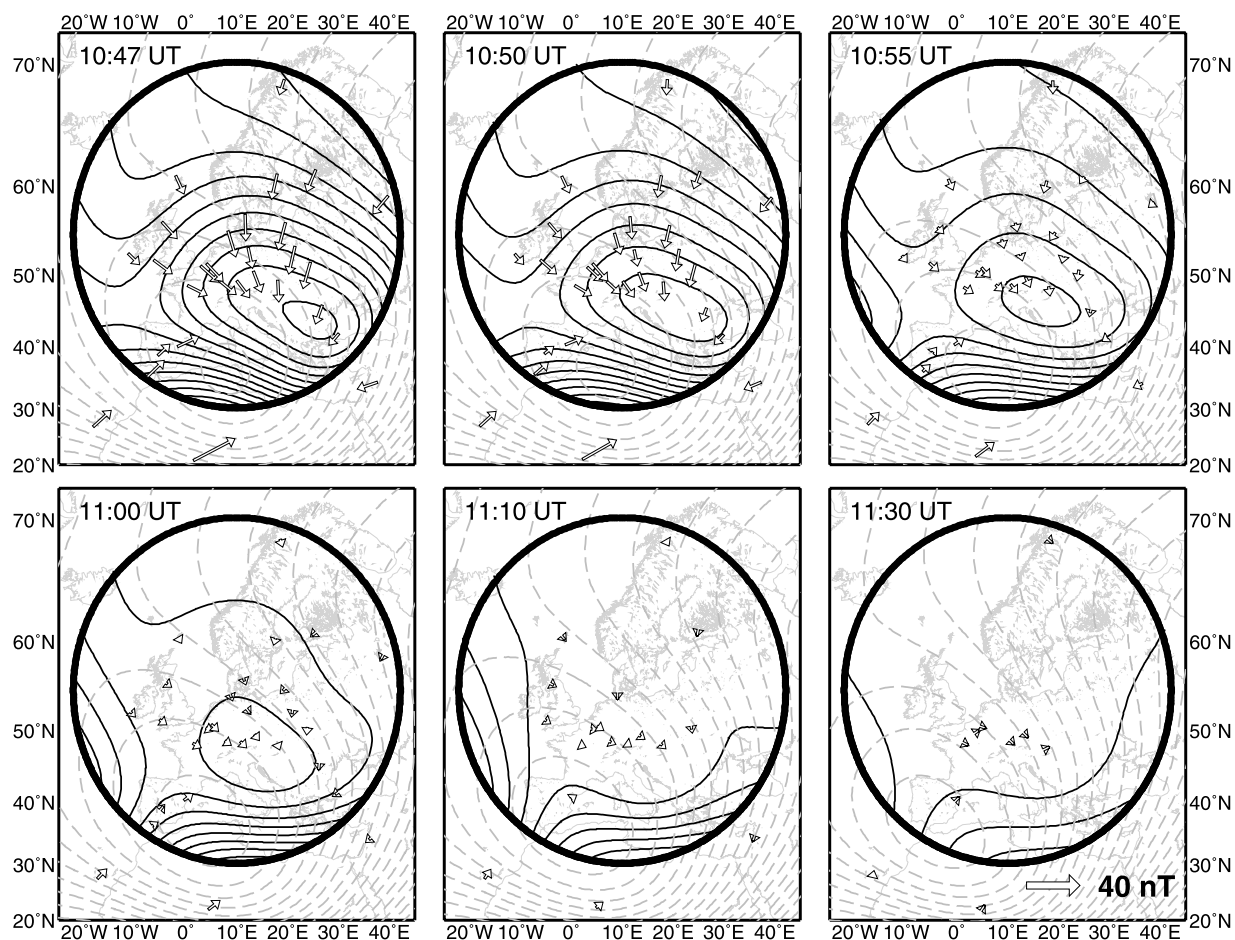
Figure 7. (continued)

[26] The size of the SFE and S_R current whorls may be determined, for instance, by measuring the size of the area encircled by the contour line whose current function value is $I = I_{max} - 25$ kA, where I_{max} is the current at the focus. Between 1034 and 1044, the size of the SFE current whorl is smaller than that of the S_R, which means that the SFE phenomenon is affected by smaller wavelengths. This justifies the use of a smaller cap for the SCHA and indicates that the external-internal separation is possibly correct. As stated by *Torta and De Santis* [1996], in the cases in which the area of existence of the variation is to some extent coincident with the cap-like region, or when some regional part of the global source can be separated (because of its independence or symmetry) from the remainder of the variation source, it is possible to carry out an SCHA of geomagnetic variations and rigorously determine their external and internal sources. In any case, there is not a model to give account for SFE external and internal magnetic variations, as they are for the Sq field, to be able to proceed with similar simulations as those presented in section 4 and be more conclusive on the above statement.

[27] The evolution of the SFE current system starts at 1026 UT with a focal point over the southern part of the studied region. The position and shape of this vortex is mainly defined by the variation recorded at Surlari observatory (SUA; 44.7°N, 26.1°E), where $\Delta X = -8.4$ nT and

$\Delta Y = -2.8$ nT for that particular instant, much sharper than for the rest of stations. These large values may be due to an anomalous local conductivity producing a strong induced field. In fact, CM4 predicts a significant bias associated to SUA (-100 nT for the horizontal components of the magnetic field). The external-internal separation given by the model might not be accurate enough at this initial moment in the vicinity of such anomalies, as the errors in the external and internal fields are equal and opposite, and a nonrealistic ionospheric current function is provided by the model at this stage.

[28] From this point afterwards, a counterclockwise vortex forms at the southeast part of the cap, gradually increasing in intensity until a maximum is reached between 1036 UT and 1041 UT. SFE vectors, especially those in southern Europe, constrain the position of the focus. It must be taken into account, as previously stated, that they represent the internal plus external variation recorded at each observatory and that the internal currents (not shown here) move the direction of the arrows southward since the focus of the internal current system is located at a lower latitude than that of the external current system. The SFE focus apparently shifts in NW direction following the oblique lines of the S_R current system. As said before, no improvement in the model was found when extending the
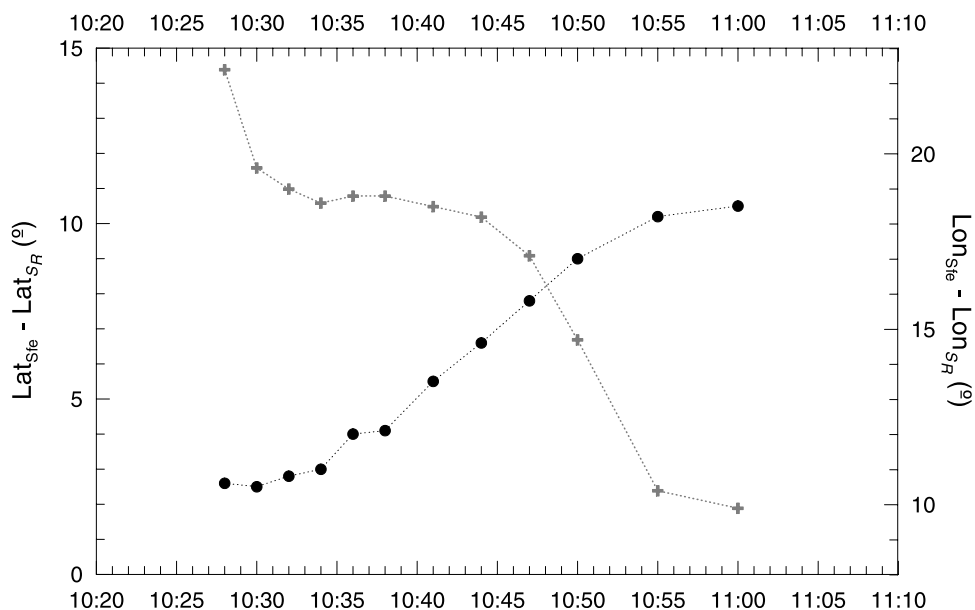
Figure 8. Temporal evolution of the difference in longitude (gray crosses) and latitude (black dots) of the SFE and S_R foci.

size of the cap southward, probably because of the lack of data for too large regions.

[29] Following this evolution, we can affirm that the SFE current system seems to form not as an enhancement of the S_R (Sq) system, but both systems present different latitude and longitude for the foci from the very beginning of the phenomenon. This would corroborate the hypothesis by *Curto et al.* [1994b] that solar flare effects are not a pure and simple increase in the diurnal variation. The center of the SFE focus appears around three degrees higher in latitude and about 1 h later in local time with respect to the focus of the S_R vortex as estimated from the SCHA model. From that point on, the difference in latitude with the S_R focus increases up to 10°, and the difference in longitude is approximately constant (the SFE focus located 10° eastward) up to 1050 UT approximately. From that moment on, the SFE focus has not such a definite structure (as can be seen from Figure 7), so it is not so obvious to obtain its location. The temporal evolution of the difference in the location between the S_R and the SFE foci is shown in Figure 8.

[30] It is worth to note that these differences are affected by errors. It does not seem feasible to allot a numerical value to the goodness of the final determination of the current system shape. The inaccuracy depends on many factors: the uncertainty derived from the analysis technique itself and its difficulty to accurately separate the external from the internal fields, the goodness of the fit to the original magnetic data, but also the procedure used to isolate the SFE signal from the recorded diurnal variation. Moreover, as said in the previous paragraph, at later times the inaccuracy in the estimation of the focus position may be larger. Nevertherless, our results are compatible with those from previous studies. By studying ten different SFE with an approximate method, *Van Sabben* [1961] found that the vortex center of the daily variation was located, on average, 6° lower in latitude with respect to the SFE focus, and almost in all cases to the west of it. *Curto et al.* [1994a]

found similar results in the global study of a particular event (1 h offset in local time and 4° shift in latitude).

[31] Our study also reflects a different inclination for both SFE and S_R elliptical current systems. According to *Curto et al.* [1994b], the action of neutral winds on the SFE current system, located at a lower altitude in the ionosphere (about 10 km lower) compared to the Sq system, makes the SFE equivalent currents to appear rotated compared to those of the Sq. The rotation is at its maximum before local noon time, when the discrepancy in the velocity of the winds for the different layers of the dynamo region is higher, translating into a phase difference at ground level between SFE and S_R variations.

[32] From 1044 UT onward, the intensity decreases progressively until the focus disappears after 1100 UT. Late undulations are due to nonzero amplitude still recorded at some observatories but, as pointed out in section 2, this could be associated to the particular interpolation adopted in the magnetograms to obtain the S_R variation. Nevertheless, it can be said that the enhancement and recovery phases are not symmetrical, the first process being much faster than the second one. This can be related to the form of the solar flux recorded by the GOES satellite and shown in Figure 1. If we assume that the focus disappears at 1110 UT, we can say that only radiation above 0.1 mW/m^2 in the 1−8 Å band produce enough ionization in order to create a prompt disturbance in the magnetic field recorded at the Earth's surface.

[33] It is worth while to remember that not all solar flares produce the same effect on the Earth's magnetic field. For example, the amplitudes of the different SFE studied by *Curto et al.* [1994a] were 30% that of the diurnal variation at peak time, whereas in our case study both amplitudes are comparable. This fact can be also seen in the similar spacing between contour lines for both vortex systems.

[34] Figure 9 shows the fit given by our model (considering internal and external coefficients) to the SFE variation
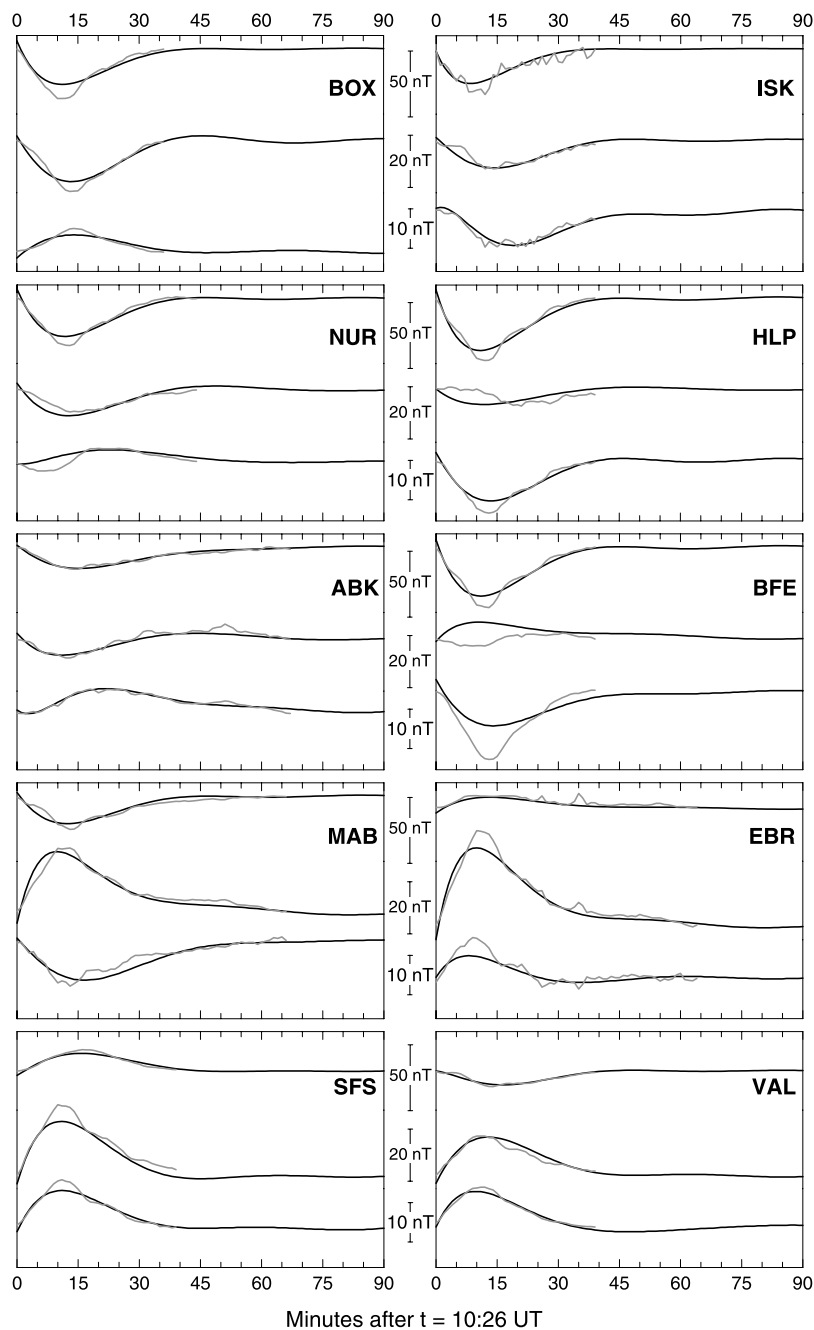
Figure 9. Temporal evolution of the SFE recorded at ten different observatories (gray lines) compared to the variation predicted by the SCHA model (black lines). Inside each box the top curve represents X component, the middle one is Y component, and the one at the bottom is the Z component. The name of each observatory is indicated by its three-character IAGA code.

recorded in the three components of the magnetic field at different observatories. It can be seen how the polynomial fit given by our model brings the variation close to zero as time passes by after the instant of maximum amplitude of the SFE. Even though the fit is quite appropriate for almost all stations both in amplitude and phase, there are some discrepancies found for five particular stations, especially regarding the fit to the phase of the event in the Y and Z components. These stations are Brofelde (BFE), Hel (HLP), Surlari (SUA), Niemegk (NGK), and Nurmijarvi (NUR). It is interesting to note that the bias predicted by the CM4

model (understood as the deviation with respect to the main field due to the local lithospheric field) for some of these observatories is very significant, as already stated for SUA. For example, the bias in the Z component for BFE given by CM4 is around −250 nT, the biases for X and Y components are close to −200 nT for HLP, and the bias in the X component for NUR exceeds 300 nT. These high values may be associated to local anomalies in conductivity as previously stated. An alternative explanation could simply be related to a nonmodeled signal, for example, due to

magnethospheric currents crossing the boundaries of the cap where the study was conducted.

6. Conclusions

[35] We have presented in this paper a new approach to study the immediate effects of solar flares on the Earth's magnetic field. We chose the particular event on 5 December 2006 because of its strength and the important disturbances it provoked. Our model allows for a simultaneous spatial and temporal interpretation of the phenomenon, improving significantly previous studies where only spatial characterization of the event for a particular snapshot was done. The spherical cap harmonic analysis technique allowed us to represent the variations recorded in the magnetic field at ground observatories as well as the ionospheric equivalent current systems responsible for these variations and for the S_R current system, demonstrating that, besides the problems associated with the technique, SCHA produced in this case a feasible internal-external separation as it was shown for the synthetic case in section 4. According to our model, the SFE equivalent current whorl is distinct from that of the S_R, its size is much smaller, and it appears to the north and around forty minutes before in local time with respect to that of the S_R, confirming previous results found by other authors for different solar flare effects.

[36] It is our hope to extend this study to other events occurring during different magnetic conditions (i.e., different parts of the solar cycle, seasons of the year, and local times), in order to conduct a systematic study of solar flare effects that will help to understand the physics behind the phenomena. The existence of an organization like INTERMAGNET provides the observatory data necessary for this kind of study in a simple and rapid way, overcoming the difficulties and delays that occurred in the past. The results will be interpreted, as done in this paper, with knowledge of all the assumptions adopted regarding the isolation of the SFE variation, and the capability of SCHA (or any other technique) to properly separate between internal and external contributions.

References

Carrington, R. C. (1859), Description of a singular appearance seen in the Sun on September 1, 1859, *Mon. Not. R. Astron. Soc.*, 20, 13–15.

Chapman, S., and J. Bartels (1940), *Geomagnetism*, vol. 2, pp. 543–1049, Oxford Univ. Press, London.

Cliver, E. W. (1995), Solar activity and geomagnetic storms: From M regions and flares to coronal holes and CMEs, *Eos Trans. AGU*, 76(8), 75–83, doi:10.1029/95EO00035.

Curto, J. J., and L. R. Gaya-Piqué (2008), Geoeffectiveness of solar flares in magnetic crochet (SFE) production: I–Dependence on their spectral nature and position on the solar disk, *J. Atmos. Sol. Terr. Phys.*, in press.

Curto, J. J., C. Amory-Mazaudier, J. M. Torta, and M. Menvielle (1994a), Solar flare effects at Ebre: Regular and reversed solar flare effects, statistical analysis (1953 to 1985), a global case study and a model of elliptical ionospheric currents, *J. Geophys. Res.*, 99(A3), 3945–3954, doi:10.1029/93JA02270.

Curto, J. J., C. Amory-Mazaudier, J. M. Torta, and M. Menvielle (1994b), Solar flare effects at Ebre: Unidimensional physical, integrated model, *J. Geophys. Res.*, 99(A12), 23,289–23,296, doi:10.1029/94JA02070.

Curto, J. J., J. O. Cardús, L. F. Alberca, and E. Blanch (2007), Milestones of the IAGA International Service of Rapid Magnetic Variations and its contribution to geomagnetic field knowledge, *Earth Planets Space*, 59, 463–471.

Futaana, Y., et al. (2008), Mars Express and Venus Express multi-point observations of geoeffective solar flare events in December 2006, *Planet. Space Sci.*, 56(6), 873–880.

Gaya-Piqué, L. R. (2004), Analysis of the geomagnetic field in Antarctica from near-surface and satellite data, Ph.D. thesis, 161 pp., Obs. de l'Ebre, Univ. Ramon Llull, Barcelona, Spain.

Haines, G. V. (1985), Spherical cap harmonic analysis, *J. Geophys. Res.*, 90(B3), 2583–2591, doi:10.1029/JB090iB03p02583.

Haines, G. V., and J. M. Torta (1994), Determination of equivalent current sources from spherical cap harmonic models of geomagnetic field variations, *Geophys. J. Int.*, 118, 499–514, doi:10.1111/j.1365-246X.1994.tb03981.x.

Hodgson, R. (1859), On a curious appearance seen in the Sun, *Mon. Not. R. Astron. Soc.*, 20, 15–16.

Kotzé, P. B. (2002), Modelling and analysis of Ørsted total field data over Southern Africa, *Geophys. Res. Lett.*, 29(15), 8004, doi:10.1029/2001GL013868.

Langel, R. A. (1993), The use of low altitude satellite data bases for modelling of core and crustal fields and the separation of external and internal fields, *Surv. Geophys.*, 14, 31–87, doi:10.1007/BF01044077.

Lowes, F. J. (1999), A problem in using spherical cap harmonic analysis to separate internal and external fields, paper presented at the XXII General Assembly, Int. Union of Geod. and Geophys., Birmingham, U. K., 19–30 July.

Ohshio, M., N. Fukushima, and T. Nagata (1967), Solar flare effects on geomagnetic field, *Rep. Ionos. Space Res. Jpn.*, 21, 77–114.

Rastogi, R. G., B. M. Pathan, D. R. K. Rao, T. S. Sastry, and J. H. Sastri (1999), Solar flare effects on the geomagnetic elements during normal and counter electrojet periods, *Earth Planets Space*, 51, 947–957.

Sabaka, T. J., N. Olsen, and R. A. Langel (2002), A comprehensive model of the quiet-time, near-Earth magnetic field: Phase 3, *Geophys. J. Int.*, 151, 32–68, doi:10.1046/j.1365-246X.2002.01774.x.

Sabaka, T. J., N. Olsen, and M. E. Purucker (2004), Extending comprehensive models of the Earth's magnetic field with Orsted and Champ data, *Geophys. J. Int.*, 159(2), 521–547, doi:10.1111/j.1365-246X.2004.02421.x.

Sastri, J. H. (1975), The geomagnetic solar flare of 6 July 1968 and its implications, *Ann. Geophys.*, 31, 481–485.

Thébault, E., J. J. Schott, and M. Mandea (2006), Revised spherical cap harmonic analysis (R-SCHA): Validation and properties, *J. Geophys. Res.*, 111, B01102, doi:10.1029/2005JB003836.

Torta, J. M., and A. De Santis (1996), On the derivation of the Earth's conductivity structure by means of spherical cap harmonic analysis, *Geophys. J. Int.*, 127, 441–451, doi:10.1111/j.1365-246X.1996.tb04732.x.

Torta, J. M., A. García, J. J. Curto, and A. De Santis (1992), New representation of geomagnetic secular variation over restricted regions by means of spherical cap harmonic analysis: Application to the case of Spain, *Phys. Earth Planet. Inter.*, 74, 209–217, doi:10.1016/0031-9201(92)90011-J.

Torta, J. M., J. J. Curto, and P. Bencze (1997), Behavior of the quiet day ionospheric current system in the European region, *J. Geophys. Res.*, 102(A2), 2483–2494, doi:10.1029/96JA03463.

Torta, J. M., L. R. Gaya-Piqué, and A. De Santis (2006), Spherical cap harmonic analysis of the geomagnetic field with application for aeronautical mapping, in *Geomagnetics for Aeronautical Safety: A Case Study in and Around the Balkans*, edited by J. L. Rasson and T. Delipetrov, pp. 291–307, Springer, Dordrecht, Netherlands.

Van Sabben, D. (1961), Ionospheric current systems of ten IGY-solar flare effects, *J. Atmos. Terr. Phys.*, 22, 32–42, doi:10.1016/0021-9169(61)90175-1.

Veldkamp, J., and D. Van Sabben (1960), On the current system of solar flare effects, *J. Atmos. Terr. Phys.*, 18, 192–202, doi:10.1016/0021-9169(60)90092-1.

Walker, J. K. (1989), Spherical cap harmonic modelling of high latitude magnetic activity and equivalent sources with sparse observations, *J. Atmos. Terr. Phys.*, 51, 67–80, doi:10.1016/0021-9169(89)90106-2.

Wessel, P., and W. H. F. Smith (1991), Free software helps map and display data, *Eos Trans. AGU*, 72(41), 441, doi:10.1029/90EO00319.

A. Chulliat and L. R. Gaya-Piqué, Équipe de Géomagnetisme, Institut de Physique du Globe de Paris, CNRS, 4 Place Jussieu, F-75005 Paris, France. (chulliat@ipgp.jussieu.fr; gaya@ipgp.jussieu.fr)

J. J. Curto and J. M. Torta, Observatori de l'Ebre, CSIC, Universitat Ramon Llull, Horta Alta 38, E-43520 Roquetes, Spain. (jjcurto@obsebre.es;